ASTRONOMY & ASTROPHYSICS
SUPPLEMENT SERIES

JANUARY I **2000**, PAGE 103

Astron. Astrophys. Suppl. Ser. **141**, 103–111 (2000)

BVRI imaging of M 51-type pairs⋆

II. Bulge and disk parameters

E. Laurikainen and H. Salo

Department of Astronomy, University of Oulu, PL 333 90571 Oulu, Finland
e-mail: eija@koivu.oulu.fi

Received September 2; accepted October 8, 1999

Abstract. We present decompositions of azimuthally averaged surface brightness profiles in optical B, V, R and I-bands for a sample of 40 M 51-type interacting galaxies. The profiles were modelled by an exponential disk and a spherical bulge described either by the $R^{1/4}$ law or by an exponential function. Half of the galaxies were well fitted by both bulge models, whereas for 35% the exponential function was a better choice. Special care was taken on eliminating superpositions of the companion galaxies. The mean B-band central surface brightness μ_0 was found to be 21.5 mag arcsec^{-2}, which is near to the value originally found by Freeman (1970), but the scatter was fairly large. Galaxy interactions have strongly modified the disks in many of the galaxies in the sample. For example, six of them had extremely flat brightness profiles outside the exponential part of the disk, and many showed significant isophotal twists.

Key words: galaxies — interactions — photometry — fundamental parameters

1. Introduction

The light distributions of the disk and bulge are generally assumed to represent physically and dynamically distinct components. While the disks are rotationally supported, the bulges are pressure supported. Well known relations are the links between the bulge-to-disk (B/D) ratio with the Hubble type (Simien & de Vaucouleurs 1986; Kent 1985) and the near constancy of the central surface brightness (Freeman 1970), although the latter has recently been suggested to be a selection effect (de Jong 1996a, 1996b). Other fundamental parameters related with the Hubble type are the effective radius and surface brightness of the bulge and disk (Simien & de Vaucouleurs 1986). All these correlations are generally suggested to manifest galaxy evolution governed by the intrinsic properties of the galaxies.

On the other hand, galaxy interactions modify galaxies affecting especially the gas distributions and the young stellar populations. For example, high surface brightness galaxies are more likely to have companions than the low surface brightness galaxies (Knezek 1993) and the central surface brightnesses of interacting galaxies are on the average higher than those of the field galaxies (Reshetnikov et al. 1993). Ellipticals located in high-density regions are characterized by smaller values of effective radii than galaxies located in the outer regions of the clusters (Strom & Strom 1978, 1979). Tidal shearing may cause sharp outer cutoffs in the brightness profiles of interacting galaxies (Chromey et al. 1998), or make the profiles systematically steeper in the outer parts with respect to the profiles of galaxies in low density regions (Bagget & Anderson 1992). Indeed, galaxy interactions may play an important role in the evolution within the Hubble sequence.

Isolated M 51-type pairs are a distinct group of interacting galaxies, where the main galaxies have rather regular morphologies and therefore the structural parameters can be well quantified. With the goal of studying the effects of interaction on the evolution of M 51-type galaxies, we present the isophotal profiles and bulge-disk decompositions for a sample of 40 galaxies. Here we describe the derivation of the bulge and disk parameters, whereas the next paper in the series will focus on the analysis.

2. The data

In order to examine the parameters describing the global structures of M 51-type galaxies 21 isolated pairs were observed in B, V, R and I passbands. The pairs were

Send offprint requests to: E. Laurikainen

⋆ Tables 1 to 4 and Figs. 2 to 4 are only available in the electronic version at http://www.edpsciences.org

selected on morphological basis, showing tidal tails and bridges and rather regular, deeply penetrating spiral arms in the main galaxy. In most of the selected pairs the companion was considerably fainter than the principal galaxy and its projected position was near the end of the bridge.

The galaxies were imaged with the 1.5 m telescope in Calar Alto, the 2.5 m Nordic Optical and 1 m Jacobus Kapteyn telescopes in La Palma, and with the 2.1 m telescope in San Pedro Martir in Baja California. In most cases the filters were in the Cousins $BVRI$ photometric system, but if r and i were in the Thuan-Gunn system they were transformed to the Cousins system. Standard reduction techniques were used to produce the calibrated images. In the final images global variations in the sky background level were comparable with the background noise, and the magnitudes reached typically the surface brightnesses of $26-27$ mag arcsec^{-2} in the B-band. A full description of the observations and data reduction, together with $B-V$ and $R-I$ color maps, can be found in Laurikainen et al. (1998) (hereafter Paper I). The analysis of one of the pairs, Arp 86, together with the N-body model has been published separately (Laurikainen et al. 1993; Salo & Laurikainen 1993).

3. Derivation of the global orientation parameters

In order to determine the disk and bulge profiles we need to estimate the orientations of the galaxies, defined by the position angle PA and inclination i. The problems related to determination of these parameters have been discussed for example by Considere & Athanassoula (1982). Both kinematic and photometric determinations are faced with problems: motions of gas in the outer parts are affected by galaxy interactions, while the inner parts might have bars or oval distortions. Also the shapes of the spiral arms might have been distorted by the interaction. Even in the case of a very detailed set of observations, like for the weakly barred galaxy IC 4214 (Buta et al. 1999), kinematic and photometric orientations may deviate by even about 10° both in PA and i; these large deviations can be explained by numerical modeling (Salo et al. 1999). In the current study two methods were used, based on visual inspection of the disk morphology:

1. Deprojection of the galaxies to face-on orientation;
2. Ellipticity of the outer contours.

Deprojection of galaxies from the plane of the sky to the face-on orientation was performed by applying an IDL routine and an example for one of the galaxies, Kar 302 A, is shown in Fig. 1. The inclination $i = 55°$ clearly is an overestimation, while $i = 45°$ is too small. The uncertainties were estimated by making deprojections with small increments in i. For some of the galaxies only an upper limit for inclination could be estimated.

Elliptical shapes of the outer isophotes were determined by fitting visually the position angle and the inclination. The fitting level was taken to be the outermost contour not showing any clear signs of perturbation by the nearby galaxy. The formal measurement errors both for the position angle and the inclination were estimated to be about 5°. As for Arp 86, also the logarithmic form of the spiral arms was used to estimate the inclination. This method gave similar or slightly smaller values than the other two methods, but it could be applied only for a few galaxies. Note that we also measured the isophotal shapes as a function of radius (see the next Sect.). However, we prefer the above subjective method in estimation of orientation, since visual inspection enables to account the effects of spiral arms and tidal deformations better than any automatic method.

The inclinations were corrected for the thickness of the disk. We used the Hubble formula for oblate spheroids and an intrinsic axis ratio of 0.2 (Aaronson et al. 1980):

$$i = \cos^{-1} \sqrt{1.024\ b^2/a^2\ - 0.042},$$

where a and b are the major and minor axis. Note that Aaronson et al. applied the additional correction term of 3° to compensate for any kinematical opening along the spiral arms: due to the reasons given by Schommer et al. (1993) the correction term was not applied here.

The estimated orientations are shown in Table 1, where the values given by De Vaucouleurs et al. (1991, hereafter RC3) are also indicated. All inclinations in the table were corrected by the above Hubble formula.

The position angles and inclinations measured at the fixed B-band surface brightness level of 25 mag arcsec^{-2} can be compared with the values given in RC3. The agreement was generally good except for some galaxies. For example, we measured PA $= 116°$ for Arp 298 B, while RC3 gives PA $= 54°$. However, our measurement is in agreement with PA $= 120°$ obtained by Marquez & Moles (1994) who used deep CCD images. For Kar 179 A a superposition of field objects has probably affected the position angle given in RC3. We also suppose that the high inclination $i = 74°$ given in RC3 for Arp 70 A may not reflect the real inclination of the disk, because the outer disk is probably strongly distorted. Our lower value $i = 50°$ for the inner regions might therefore be more realistic.

4. Isophotal shapes and azimuthally averaged brightness profiles

4.1. Isophotal shapes

The radial brightness variations were analysed by fitting ellipses to the isophotes of the surface brightnesses. For this purpose an IDL program was developed, based partially on the Fourier-technique as used by Kent (1983), Jedrzejewski (1987) and Rauscher (1995). The basic difference is that we first determined a good initial

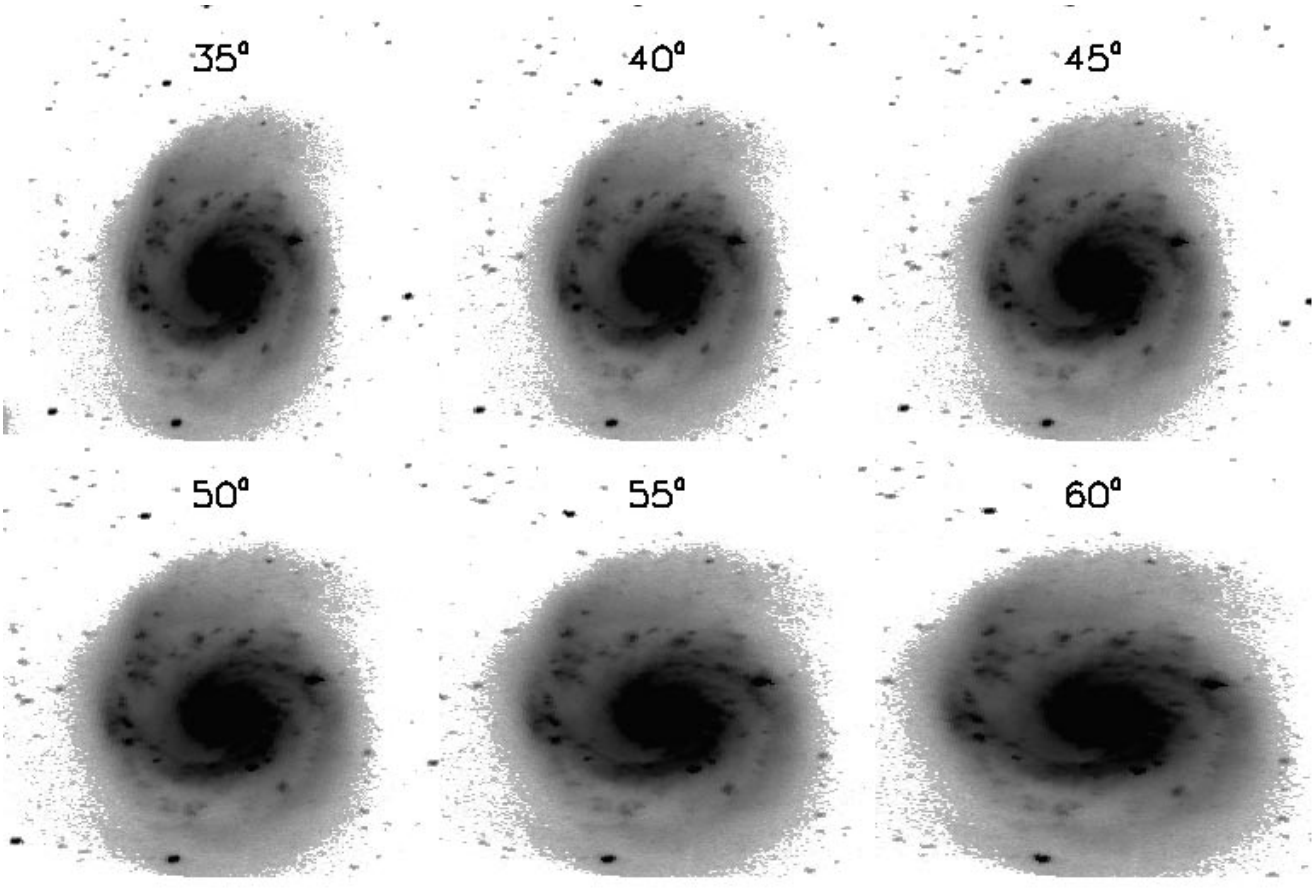

Fig. 1. Kar 302 A (I-band) deprojected to the face-on orientation using the position angle PA = 170° and inclinations i = 35°, 40°, 45°, 50°, 55° and 60°. The galaxy brightness is shown in the logarithmic scale

fit by choosing a fixed brightness level and finding the best ellipse to fit the image points at this level (method I), and only then proceeded with the Fourier-technique
(method II).

I) Our IDL routine starts by choosing image points corresponding to a fixed brightness level. These points are fitted by an ellipse, defined by its center (x_c, y_c), major and minor axis radii (a, b), and major axis position angle. The fitting is done with a general least squares iteration that minimizes the sum

$$g = \sum (x_p - x_e)^2 - (y_p - y_e)^2,$$

where x_p and y_p are the image points, and x_e and y_e are the corresponding nearest points in the fitting ellipse. The fit is further polished by accepting only those pixels within 3 standard deviations from the fitted ellipse. In the program two options to select the isophote pixels are available: automatic selection within the range of the tolerance (typically 2% of the specified brightness level) or manual selection by indicating the acceptable parts of the image with mouse. The manual option is valuable for example when fitting isophotes which are strongly affected by the spiral arms in the outer parts of the galaxy. Also, in the inner parts where fewer pixels fall into the tolerance interval, we use bilinear interpolation to create at least 50 points corresponding to the given surface brightness level.

II) Once a good initial fit is obtained as described above, the program proceeds with the intensity-fit technique of Jedrzejewski (1987). It thus fixes the semimajor-axis a and fits the intensity along the ellipse with the function

$$I = I_0 + A_1 \sin(E) + B_1 \cos(E) + A_2 \sin(2E) + B_2 \cos(2E),$$

where E is the eccentric anomaly used to parametrize the points of the ellipse. Intensity in these sample points is calculated with bi-linear interpolation. The ellipse parameters x_c, y_c, b and PA are iteratively corrected according to the coefficients A_1, A_2, B_1 and B_2 and the intensity gradient along the major axis, until a good fit to I = constant is found. The criterion to stop the iteration is that the largest harmonic amplitude is less than 4% of the rms residual intensity along the ellipse. If no convergence is found, as often happens in the outer portions of the image where the intensity gradient is small, the ellipse parameters of the initial fit are taken as final values.

The error estimate for the fit parameters is made in the same manner as in Rauscher (1995), namely from the

errors in harmonic coefficients and the rms residual of the intensity. This error estimate is also used in the case the intensity-fit (method II) fails to converge, by applying Rauscher's error formulas for the initial fit obtained by method I.

We have tested our algorithm by measuring the position angle and ellipticity variations for NGC 4303 (using our high-resolution IR-data) and by comparing them with the published IR measurements by Rauscher (1995). We obtained reasonable ellipticities and position angles with small error bars for the whole image region ($r < 30$ arcsec), whereas Rauscher reports good measurements only for the inner 3 arcsec, where our measurements are identical to their values. The reason for the difference is that, in contrast to our combined methods, Rauscher's method fails when no good initial guess is available. Comparison to the IRAF program "ellipse" was made using the B-band image of NGC 5905: similar results were obtained except that "ellipse" gave slightly smaller error bars than our program. The program "ellipse" is also based on the same Rauscher's method. We also tested our algorithm with the B and H-band data of the weakly barred galaxy IC 4214 (Buta et al. 1999), obtaining practically identical results as compared to the program SPRITE developed at the University of Alabama.

The isophotal parameters are shown in Fig. 2. Also marked are the PA and the ellipticity $\epsilon = 1 - b/a$, corresponding to our visual estimates of galaxy orientations. In most cases the visual estimations correspond to the averaged PA values in the outer parts of the disks, but there are a few exceptions for which the visually estimated value is different. For Kar 331 A this difference can be explained by a bright object in the galaxy area, whereas for Kar 296 A and NGC 5905 open spiral arms affect the automatic measurement.

4.2. Azimuthally averaged profiles

For computing the intensity profiles the standard approach was followed. Instead of fitting ellipses to the isophotes, fixed inclination and position angle were used and the mean intensities were calculated in elliptical annuli evenly distributed in radius. The algorithm included automatic elimination of foreground stars. Identification of the data points contaminated by star light was based on pixel values exceeding the mean value in the annulus at least by 2-4 standard deviations, depending on the image.

Interacting galaxies have the additional problem that they are sometimes superimposed by the nearby galaxies. Therefore the fitting routine includes the possibility to compensate the affected data points with the mean values of the good pixels in the same annulus. The excluded area is specified by radius and position angle intervals.

Figure 3 shows the measured azimuthally averaged profiles. No corrections for Galactic or internal extinction or seeing were applied. The sources of error in the surface brightnesses were taken to be the background noise and the global variations in the sky level, taken to be the difference between the minimum and maximum sky brightnesses divided by four. The latter is somewhat smaller than used for example by de Jong (1996b), but on the basis of our tests with synthetic data it is still probably an overestimation for the true uncertainties due to sky variations.

In the literature deep intensity profiles were found for three galaxies common with our sample: NGC 5905, Arp 87 A and Kar 302 A. For NGC 5905 our profiles were identical with the B, V and R profiles by Wozniak et al. (1995), whereas in the I-band there was a half magnitude shift, which may be related to the large amount of processing of the I-image by them: Wozniack et al. had strong interference fringes in the I-frame so that additional correction frames had to be used. The comparison was made to the surface brightness level of 24 mag arcsec^{-2} in the B-band. For Arp 87 A our V-profile was identical with that by Gavazzi & Randone (1994) who had the same limiting surface brightness as we did. Also, for Kar 302 A our I-profile was identical with the profile by Heraudeau & Simien (1996) to the distance of about 80 arcsec, after which there was a half magnitude shift. This shift is most probably caused by uncertainties in the sky subtraction. We note that both Arp 87 A and Kar 302 A were observed during the run in Calar Alto in 1992, for which campaign an additional correction of 0.6 mag to the zero points was applied in Paper I. The correction was done by comparing with the magnitudes in RC3, which are generally based on lower quality data than the above CCD- observations by Wozniak et al. and Gavazzi and Randone. Therefore the correction applied in Paper I should NOT be applied. In the literature intensity profiles can be found also for Arp 298 A, Kar 125 A and B and NGC 5908 (Kotilainen et al. 1993; Marquez & Moles 1996; de Robertis et al. 1998), but as their data occupy only the high surface brightness parts of the profiles no comparisons were done.

Table 2 provides information similar to that generally given in galaxy catalogues. R_{25} is the radius and m_{25} the integrated apparent magnitude measured within the isophote having a surface brightness of $\mu_B = 25$ mag arcsec^{-2}. The parameters $r_{\rm e}$ and $\mu_{\rm e}$ are the effective radius and surface brightness in units of arcsec and mag arcsec^{-2}, respectively. Also shown are the total integrated apparent magnitudes and the B-band absolute magnitudes after correcting for redshift and Galactic extinction. The standard correction terms are from RC3. Internal extinction corrections are much more difficult to assess and were not considered. The total magnitudes were in most cases derived by extrapolating the exponential profiles to infinity. However, as some of the galaxies had flat regions outside the exponential parts of the profiles this extrapolation was not done. Note that the total magnitudes in Table 1 are not necessarily the same as in Paper I

(its Table 4), where the magnitudes were measured by single apertures without correcting for the superpositions of the nearby galaxies or extrapolation to infinity.

The error bars for μ_e were estimated from the global variations in the sky level and by taking into account the background noise, whereas for R_{25} and r_e they were estimated from the uncertainties in the surface brightnesses. The error limits for integrated magnitudes include the magnitude zero-point errors and the background noise.

The R_{25} radii in the B-band were compared with the values given in RC3. Our measurements did not show any systematic shift as compared to the RC3 values, but measurements for individual galaxies in many cases disagreed, typically by $5-30\%$. One of the cases with large difference was NGC 5905, for which we obtained $R_{25} = 89''$ whereas RC3 gives $R_{25} = 119''$. The value we obtained is reasonable, because our profile was identical with that measured by Wozniak et al. (1995) in the region common with their measurement. In general CCD-images are a more accurate way of measuring the bulge and disk parameters than the aperture photometry often used in RC3.

5. Bulge-disk decomposition

5.1. The model components

Galaxy surface brightness profiles are generally well represented by an exponential disk and a spherical bulge, although bars, ovals, star forming regions and thick disks may cause additional structures (Bahcall & Kylafis 1985; Bagget et al. 1998 and references therein). The formula for the exponential light profile in flux units is:

$$\Sigma(r) = \Sigma_0 \exp(r/h),$$

and in magnitudes:

$$\mu(r) = \mu_0 \ + \ 1.068 r/h,$$

where Σ_0 is the central surface intensity (μ_0 in magnitude units) and h is the scale length. Characteristic for the Freeman type II (Freeman 1970) profile is that the data dips below the exponential model. In fact, Kormendy (1977) first showed that at least empirically the inner-truncated exponential function can better fit this kind of profiles. Recently truncated exponentials have been successfully applied to several spiral galaxies by Bagget et al. (1998). Therefore we also used the inner truncated exponential of the form:

$$\Sigma(r) = \Sigma_0 \exp\ (-r/h \ - \ (r_h/r)^n),$$

where r_h is the radius of the central cutoff of the disk and $n = 3$ as suggested by Kormendy (1977).

Successful fits to the bulges of spiral galaxies have been obtained by Hubble law (Hubble 1930), King model (King 1966), de Vaucouleurs $R^{1/4}$ law (de Vaucouleurs 1948), by a generalized version of de Vaucouleurs' law $R^{1/n}$ (Caon et al. 1993; Andreakis et al. 1995) and by an exponential function (Kent et al. 1991; Andreakis & Sanders 1994; Bagget et al. 1998). Kormendy has shown that for elliptical galaxies the Hubble, King and $R^{1/4}$ models describe approximately the same physical quantities. The most generally used function for bulges is the $R^{1/4}$ law, but exponential functions have also been largely applied. In order to better compare with the bulge-disk decompositions presented for spiral galaxies by other authors we applied both the $R^{1/4}$ law and the exponential function. The $R^{1/4}$ law takes the form of:

$$\Sigma(r) = \Sigma_e \exp(-7.67\ [(r/r_e)^{1/4} - 1]),$$

$$\mu(r) = \mu_e \ + \ 8.325[(r/r_e)^{1/4} - 1],$$

where Σ_e is the effective surface intensity (μ_e in magnitudes) and r_e the effective radius of the bulge.

A less commonly used function to fit the brightness profiles of the bulges, but often used in dynamical galaxy models, is the Plummer sphere with projected surface density

$$\Sigma(r) = \Sigma_p \ / \ (1 + (r/h_p)^2)^2,$$

which was here applied for testing purposes (for Plummer sphere $r_e \approx 1.3\ h_p$ and $\Sigma_e \approx 0.29\Sigma_p$).

5.2. Fitting procedure

Our method of decomposing the bulge and disk components in the luminosity profiles resembles the procedure first advocated by Kormendy (1977) and later by Boroson (1981). The initial parameters of the profiles are first guessed after which the program iteratively solves the parameter values. The fitting to the data was accomplished by minimizing the weighted rms deviation of the data from the fit:

$$\chi^2 = \sum \ w_i \ (\Sigma_i - \Sigma_{\rm fit})^2,$$

where Σ_i and $\Sigma_{\rm fit}$ denote the measured and modelled surface brightnesses. The main difference to Boroson (1981) is that here the fits to the bulge and disk are made simultaneously, rather than attempting to decompose with successive pairwise iterations. The IDL-routine "curfit" was applied: it uses gradient-expansion algorithm to compose a non-linear least squares fit to a user supplied function. Iterations were performed until the chi-square changed by less than 0.1%.

The weighting function to the data points can be selected either on the purposes to give more weight to the inner portions where the intensities are high or to the lower surface brightnesses describing larger areas, both alternatives being equally well motivated. A commonly used weighting function uses the variance of the intensity measurement as the basis, with the weight of the $i^{\rm th}$ point being:

1. $w_i = 1/\sigma_i^2$,

where σ_i^2 is the variance of the $i^{\rm th}$ point (Bevington 1969). For Poisson statistics $\sigma_i^2 \propto \Sigma_i$ and we use consequently $w_i = 1/\ \Sigma_i$. This weighting function has been used for example by Bagget et al. (1998) and by de Jong (1996a), while in most studies the used weighting function has not been stated.

In order to test the effects of different weighting functions on the bulge and disk parameters three other choices were applied:

2. w_i = constant,

3. $w_i = 1/\Sigma_i^2$,

4. $w_i = 1/\Sigma_{\rm annulus}$,

where $\Sigma_{\rm annulus}$ is the total flux within each measured elliptical annulus in the profile. The first and the third weighting functions give more weight to the lower surface brightnesses, whereas the second and fourth functions stress the inner parts of the profile. We also performed unweighted fits in magnitude units, corresponding to $\chi^2 = \sum (\mu_i - \mu)^2$. The fit performed with the function $w_i = 1/\Sigma_i^2$ applied to the data in flux units closely corresponds to the fit performed in magnitude units.

The effects of various weighting functions were studied by running the bulge-disk decomposition routine for a few high quality brightness profiles (NGC 5908 and Arp 87 B) by applying all the above weighting functions. The decomposition routine was first applied to the original data and then to the profiles in which noise ($10\% - 30\%$) was added and then the two measurements were compared. The best weighting function, in a sense that it resulted in the smallest variation between the two measurements, was $w_i = 1/\Sigma_i^2$. While applying the fits to the data in magnitude units without any weighting function, even more stable results were obtained. In this study the last alternative was used.

To account for the effects of seeing the model profiles were convolved with a Gaussian Point Spread Function (PSF) by using the dispersion σ measured from the foreground stars for each individual frame (see Table 3, Col. 3). The azimuthally averaged profile, convolved by seeing, can be described as:

$$\Sigma_{\rm s}(r) = \sigma^{-2} \exp(-r^2/2\sigma^2)$$
$$\int \Sigma(x) I_0(xr/\sigma^2) \exp(x^2/2\sigma^2) x {\rm d}x$$

where $\Sigma(r)$ is the intrinsic surface brightness profile, σ the dispersion of the Gaussian PSF and I_0 the zero-order modified Bessel function of the first kind (Pritchet & Kline 1981). Eventhough seeing affects most heavily the bulge, our algorithm applies correction also for the disk model functions.

To get an estimate of the goodness of the fit we used the unweighted magnitude residuals:

$$\triangle^2 = \sum\ (\mu_i - \mu_{\rm fit})^2\ /\ N,$$

where μ_i is the profile value, $\mu_{\rm fit}$ the calculated fitted value and N is the number of data points.

5.3. Fitting the data

The following combinations of the fitting functions were applied:

1. de Vaucouleurs' bulge + exp. disk (model 1),

2. exp. bulge + exp. disk (model 2),

3. de Vaucouleurs' bulge + truncated exp. disk (model 3),

4. exp. bulge + inner truncated exp. disk (model 4), and

5. Plummer bulge + exp. disk (model 5).

The models 1 and 2 were applied for most of the galaxies and the resulting parameter values for the bulge and disk are shown in Tables 3 and 4. No corrections for inclination or Galactic or internal extinction were applied. The parameters characterizing the disk are the central surface brightness μ_0, the scale length h and the effective surface brightness and radius $\mu_{\rm e}$ and $r_{\rm e}$ (on the left in the tables), while the bulge is characterized by the effective parameters $\mu_{\rm e}$ and $r_{\rm e}$ (on the right in the tables). Also the resulting bulge-to-disk total flux ratio B/D is shown. Before decomposing the brightness profiles they were generally rebinned outside the bulge regions. Some of the profiles showed strong deviations from exponential disks having bumps above the theoretical profiles. This kind of profiles were fitted by excluding the strong structures. The structures are probably caused by vigorous star formation or by some other component not part of the flat disk, so that excluding them probably made the rms deviations to better reflect quality of the fits to the true disks. We noticed in Sect. 4.2 that some of the profiles were extremely flat in the outer portions. This kind of flat profiles cannot be modelled for example by a second exponential function, because that would cause infinitely large disks. Therefore we decided to exclude the flat outer parts from the profile fits. Some of the images of Arp 296 were saturated in a few nuclear pixels so that the innermost parts of their profiles were excluded from the fit. The decomposition was not applied for NGC 5908 seen almost edge-on, because deprojecting the galaxy to face-on would artificially stretch the spherical bulge.

The bulge-disk decompositions are presented in Fig. 4 so that only the best fitting decompositions, generally in the R-band, are shown. The seeing effect has been discussed in detail by Bagget et al. (1998) who pointed out that the errors due to seeing largely depend on the size of the seeing disk compared with the parameters of the fits. According to them the effective radius changes $1\% - 40\%$ when seeing has been changed $1 - 7$ arcsecs. In our case,

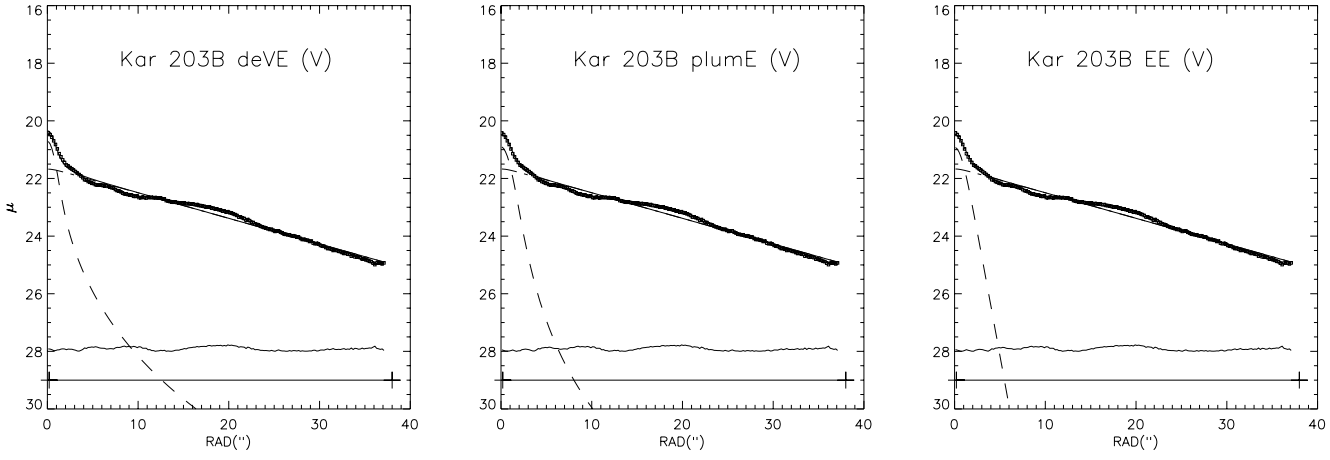

Fig. 5. Comparison of the bulge-disk decompositions with different bulge models for Kar 203 B in the V-band: the $R^{1/4}$ law (deV), Plummer bulge (Plum) and an exponential function (E)

for example, without correcting the 1.5 arcsec seeing observed for Arp 87 B, would cause 10% error to the effective radius for both the bulge and the disk, 3% error to the scale length, and less than 1% error to the central surface brightness of the disk.

5.4. Error analysis

5.4.1 Measurement errors

The most important source of error was the global variations in the sky brightnesses. These uncertainties were estimated by adding the sky level error (estimated as explained in Sect. 4.2) to the original profiles and the measurements were repeated. The differences of the two measurements then gave the errors shown in Table 5. The errors were measured for all profiles, while in the table only the mean values in each band for the two bulge models are shown. As expected, the central and effective surface brightnesses are barely affected, and the uncertainties for the effective radii of the disk are similar for the two bulge models. The errors for the effective radii of the bulge are $5-10$% by model 1, while by model 2 they are only half of that. Also, the uncertainties of the B/D ratio are higher when model 1 is applied.

The zero-point errors of the flux calibration were $0.009-0.1$ mag arcsec^{-2} so that their contribution to the bulge and disk parameters are negligible.

5.4.2 Fitting errors

The standard deviations of the fits were considerably smaller than for example the uncertainties due to sky variations. In fact, a more useful way of estimating quality of the fits is to look at the values of the unweighted rms residuals. By taking the mean $\triangle$ for all the fits performed by one method a quite small mean value $<\triangle>=0.12\pm0.05$ mag was obtained. The bulge model used did not affect the result. Also, while excluding bad fits from the statistics the mean $\triangle$ was not significantly changed.

The effect of the weighting function to the bulge-disk decomposition has not been previously studied although it may contribute significantly to the uncertainties of the derived parameters. We applied all the weighting functions explained in Sect. 5.2 to the brightness profiles of NGC 5908 and Arp 87 B and compared the measured parameter values to those obtained by the fits made to the unweighted data in magnitude units. For the central surface brightnesses the resulting relative differences were less than 1.5%. However, for the scale lengths the weighting function was more important: depending on the function applied the difference varied between $0.5-20$%, and as expected were smallest for the weighting function $w_i = 1/\Sigma_i^2$.

5.4.3 Comparison of the models

Our third estimate of the decomposition uncertainties was to compare the fits performed by the two bulge models, $R^{1/4}$ law and the exponential function. The comparisons in the B-band are shown in Table 6, where the mean parameter values with their standard deviations are shown. In the comparison only those galaxies were used for which good fits were obtained by both bulge models.

It is obvious that changing the bulge fitting model affects mostly the parameters of the bulge, while the parameters of the disk are maintained rather similar. Indeed, mean r_e for the bulge was affected even 4.2 arcsec, the fitting model thus being the largest source of uncertainty for this parameter. The bulge model was less important for the parameters of the disk, for example, the central and effective surface brightnesses were hardly affected. The B/D ratio was most dramatically affected, which is well understandable, as the $R^{1/4}$ law function extends to a much larger radii than the exponential function. This is demonstrated for Kar 203 B in Fig. 5, where the application of the Plummer bulge is also shown. In fact, the Plummer bulge could for some cases be a very reasonable choice, especially for galaxies with rather large bulges.

Table 5. Uncertainties in the derived parameters due to sky variation error

Filter	$\Delta\mu_0$	Δh	$\Delta m\mu_e$	$\Delta\mu_e$	Δr_e	$\Delta m\mu_e$	$\Delta\mu_e$	Δr_e	$\Delta\ (B/D)$
model 1									
B	0.10	0.35	0.10	0.10	0.43	0.12	0.10	0.88	0.21
V	0.05	0.21	0.07	0.06	0.30	0.12	0.13	0.53	0.13
R	0.04	0.14	0.06	0.04	0.21	0.05	0.06	0.45	0.07
I	0.07	0.27	0.08	0.08	0.51	0.05	0.05	0.46	0.14
model 2									
B	0.10	0.57	0.09	0.09	0.74	0.05	0.06	0.13	0.05
V	0.06	0.29	0.06	0.06	0.42	0.07	0.07	0.13	0.01
R	0.03	0.17	0.03	0.05	0.26	0.02	0.04	0.08	0.07
I	0.07	0.32	0.06	0.06	0.47	0.02	0.03	0.07	0.02

Table 6. Comparison of models 1 and 2 in B-band

Parameter	model 1	model 2
μ_0 (disk)	21.5 ± 0.7	21.5 ± 0.7
h (disk)	7.9 ± 4.3	8.8 ± 4.2
$m\mu_e$ (disk)	21.9 ± 0.7	21.8 ± 0.6
μ_e (disk)	23.3 ± 0.7	23.2 ± 0.6
r_e (disk)	13.0 ± 7.2	14.3 ± 6.8
$m\mu_e$ (bulge)	21.0 ± 1.3	19.9 ± 1.1
μ_e (bulge)	23.0 ± 1.3	21.3 ± 1.1
r_e (bulge)	6.7 ± 4.7	2.5 ± 1.6
B/D	0.9 ± 0.7	0.3 ± 0.3

5.5. Comparison with previous bulge-disk decompositions

Bulge-disk decompositions for Arp 70 A and B, Kar 64 A and B, and Arp 298 B, common with our sample, have been made by Reshetnikov et al. (1996) in the R-band by applying the $R^{1/4}$ law for the bulge and an exponential function for the disk. Their fitting method is similar to ours, but contrary to us they did not apply any seeing correction or try elimination of the contributions of the companion galaxies to the brightness profiles. For Arp 298 B the profile by Reshetnikov et al. (1996) does not extend to the exponential part of the disk so that comparison was not made. For the galaxies Arp 70 A and B both μ_0 and h for the disk and μ_e for the bulge determined by us were quite different from their values. For example, for Arp 70 A Reshetnikov et al. give $\mu_0 = 23.1$, $h = 12.9$ and $\mu_e = 22.1$, whereas we obtained $\mu_0 = 20.1$, $h = 5.8$ and $\mu_e = 21.6$. Evidently the differences, especially for the disk scale length and the central surface brightness, are very large. The reason to the difference is that while Reshetnikov et al. fitted the whole observed profile, we used only the non-flattened part of the profile. We remind that Arp 70 A is one of those galaxies in our sample which has nearly constant surface brightness outside the exponential part of the disk. For Kar 64 A and B our fitting regions were considerably larger than those by Reshetnikov et al. This together with the seeing effect may explain the small differences between the two bulge-disk decompositions. It is also worth noticing that contamination by the light of the companion mainly affects the lower surface brightnesses and therefore can modify the parameters derived for exponential disks.

Bulge-disk decompositions for the galaxies Kar 125 A and Arp 298 A have been performed by Marquez & Moles (1996) and by Kotilainen et al. (1992), but as their data do not cover the exponential parts of the disks no comparison was made.

6. Summary

We have presented azimuthally averaged radial brightness profiles and isophotal shapes for 40 M 51-type interacting galaxies in B, V, R and I bands. Also, in order to quantify the characteristics of the bulge and disk components, bulge-disk decompositions were performed. Three of the galaxies, Arp 298 A, Arp 218 A and Kar 203 A, show Freeman type II profiles. This kind of galaxies often have outer rings (Bagget et al. 1998) which is the case also for the Seyfert galaxy Arp 298 A. On the other hand, Kar 203 A is a peculiar galaxy for which the Freeman type II profile is most probably related to the extremely bright, almost point-like source near to the nucleus.

Most of the galaxies in our sample have typical surface brightness profiles with a nearly exponential outer disk, but quite many of them also showed peculiar characteristics. Namely, six of the galaxies, Arp 70 A and B, Arp 82 A and B, Arp 87 A and Kar 404 A had flat brightness

profiles outside the normal exponential disks so that in the flat regions the surface brightnesses were almost constant between $\mu_0 = 25 - 26.5$ mag arcsec^{-2}. All these galaxies belonged to the category of the prototypical M 51-type pairs where a small companion resides at the very end of the bridge. The flat profiles appeared prefentially in the main galaxies, but in two cases also the profiles of the companion galaxies were flattened. The flat profiles consisted of 16% of all the profiles studied, and even 26%, if only M 51-type pairs in a more limited sense were considered. In this kind of pairs the interaction has clearly strongly modified the galactic disks thus probably playing an important role in their evolution. Low surface brightness extensions in the brightness profiles have been previously reported by Bagget et al. (1998) in about 2.7% (18 galaxies) of the galaxies in their spiral galaxy sample. The flat profiles found by us are quite different than for example the profile of the strongly interacting galaxy NGC 3628 which has a sharp outer cutoff just before the flat part of the disk (see Chromey et al. 1998). Also, isophotal twists were detected in many of the galaxies studied.

We used the profile decomposition method where fitting to the data was accomplished by minimizing the weighted rms deviation of the data from the model profile and where a seeing correction to the theoretical profiles was applied. Special attention was paid on eliminating the effects of the nearby galaxies on the brightness profiles. The disks were well represented by exponential functions in all cases expect for three galaxies which had Freeman type II profiles. The bulges were approximately equally well represented both by the $R^{1/4}$ law and an exponential function for 51% of the profiles, while an exponential bulge explained better 35% of the cases. Only for 5% (NGC 5905 and Arp 298 B) a better fit was obtained by the $R^{1/4}$ law. Andreakis & Sanders (1994) have found for a large sample of normal spiral galaxies that exponential bulges generally appear in late-type spirals. However, here no clear correlation between the fitting model and the morphological type of the galaxy was found.

The mean central surface brightness of the disk in B-band was found to be 21.5 mag arcsec^{-2}, regardless of the bulge function applied, which is very near to the value of 21.6 mag arcsec^{-2} originally obtained by Freeman (1970). However, the scatter was large the central surface brightness varying between 19 and 22.7 mag arcsec^{-2}. This confirms the result by de Jong (1996b) showing that μ_0 actually is not a constant, rather there is only an upper limit for this quantity. We also found that the weighting function is not an unimportant factor in the bulge-disk decompositions. It affects mostly the scale lengths so that the uncertainty in the worst case can be even 20%.

Acknowledgements. We thank the referee Dr. Florence Durret for her valuable comments.

References

Aaronson M., Mould J., Huchra J., 1980, ApJ 237, 655
Andreakis Y.C., Sanders R.H., 1994, MNRAS 267, 283
Andreakis Y.C., Peletier R.F., Balcells M., 1995, MNRAS 275, 874
Bahcall J.N., Kylafis N.D., 1985, ApJ 288, 252
Bagget W.E, Anderson K.S.J., 1992, AJ 103, 436
Bagget W.E., Bagget S.M., Anderson K.S.J., 1998, AJ 116, 1626
Bevington P.R., 1969, Data Reduction and Error Analysis of the Physical Sciences. New York, McGraw Hill
Boroson T., 1981, ApJS 46, 177
Buta R., Purcell G.B., Lewis M., Crocker D.A., Rautiainen P., Salo H., 1999, AJ 117, 778
Caon N., Cappaccioli M., D'Onofrio M., 1993, MNRAS 265, 1013
Chromey F.R., Elmegreen D.M., Mandell A., McDermot J., 1998, AJ 115, 2331
Considere S., Athanassoula E., 1982, A&A 111, 28
de Jong R.S., 1996a, A&AS 118, 557
de Jong R.S., 1996b, A&A 313, 45
de Robertis M.M., Hayhoe K., Yee H.K.C., 1998, ApJS 115, 163
de Vaucouleurs G., 1948, Ann. Astrophys. 11, 247
de Vaucouleurs G., de Vaucouleurs A., Corwin H.G., Buta R., Paturel G., Fouqué P., 1991, The Third Reference Catalogue of Bright Galaxies. Springer-Verlag, New York (RC3)
Freeman K.C., 1970, ApJ 160, 811
Gavazzi G., Randone I., 1994, A&AS 107, 285
Heraudeau Ph., Simien F., 1996, A&AS 118, 111
Hubble E., 1930, ApJ 71, 231
Jedrzejewski R.I., 1987, MNRAS 226, 747
Kent S.M., 1983, ApJ 266, 562
Kent S.M., 1985, ApJS 59, 115
Kent S.M., Dame T., Fazio G., 1991, ApJ 378, 131
King I.R., 1966, AJ 71, 64
Knezek P., 1993, Ph.D. Thesis, Univ. Massachusetts
Kormendy J., 1977, ApJ 217, 406
Kotilainen J.K., Ward M.J., Boisson C., De Poy D.L., Bryant L.R., Smith M.G., 1992, MNRAS 256, 125
Kotilainen J.K., Ward M.J., Williger G.M., 1993, MNRAS 263, 655
Laurikainen E., Salo H., Aparicio A., 1993, ApJ 410, 574
Laurikainen E., Salo H., Aparicio A., 1998, A&AS 129, 517 (Paper I)
Marquez I., Moles M., 1994, AJ 108, 90
Marquez I., Moles M., 1996, A&AS 120, 1
Pritchet C., Kline M.I., 1981, AJ 86, 1859
Rauscher B.J., 1995, AJ 109, 1608
Reshetnikov V.P., Hagen-Thorn V.A., Yakovleva V.A., 1993, A&A 278, 351
Reshetnikov V.P., Hagen-Thorn V.A., Yakovleva V.A., 1996, A&A 314, 729
Salo H., Laurikainen E., 1993, ApJ 410, 586
Salo H., Rautiainen P., Buta R., et al., 1999, AJ 117, 792
Schommer R.A., Bothun G.D., Williams T.B., Mould J.R., 1993, AJ 105, 97
Simien F., de Vaucouleurs G., 1986, ApJ 302, 564
Strom K.M., Strom K.M., 1978, AJ 83, 1293
Strom K.M., Strom K.M., 1979, AJ 84, 1091
Wozniak H., Friedli D., Martinet L., Martin P., Bratschi P., 1995, ApJ 111, 115